Available online at www.sciencedirect.com
SCIENCE DIRECT®
Polymer 45 (2004) 2465–2473
polymer
www.elsevier.com/locate/polymer

Study of the water uptake of polyamide 46 based copolymers by magnetic resonance imaging relaxometry

Peter Adriaensens[a], Anne Pollaris[a], Rudy Rulkens[b], Victor M. Litvinov[b], Jan Gelan[a,*]

[a]*Limburgs Universitair Centrum, IMO, Division Chemistry, Universitaire Campus, B-3590 Diepenbeek, Belgium*
[b]*DSM Research, P.O. Box 18, 6160 MD Geleen, The Netherlands*

Received 12 August 2003; received in revised form 9 February 2004; accepted 9 February 2004

Abstract

Magnetic resonance imaging (MRI), NMR relaxometry, thermal analysis and gravimetrical experiments are performed to study the water absorption by neat PA46 and copolymers of PA46 and PA4n (PA46-*co*-PA4*n*) with 4 mol% $n = 8$, 12 and 16. The observed reduction in water uptake, ingress rate and water molecular mobility with increasing value of n is explained by a combination of several physico-chemical molecular properties. The increased [CH_2]/[amide] ratio and the reduced amount of crystallinity do not completely clarify the observed trends in water uptake and water molecular mobility in the copolymer series. It is shown that the increased chain mobility of the PA46 segments in the copolymers allows an improved coupling of the amide groups in the amorphous phase, explaining the observed decrease in water uptake. The important role of the morphology of the amorphous phase for water uptake is further demonstrated by annealing results and NMR relaxation experiments as a function of temperature.

Keywords: MRI; Relaxometry; PA46 copolymers

1. Introduction

Polyamide 46 (poly-tetramethylene adipamide, PA46), a specialty high performance polyamide made from tetramethylenediamine and adipic acid, was first synthesized by Carothers as early as 1938 [1]. It took until 1977, before Gaymans [2] developed a procedure to obtain sufficiently high-molecular-weight PA46 without discoloration. Currently PA46 is a commercial product of DSM with the trade name Stanyl®. The large number of amide groups per unit length of chain, combined with the highly symmetrical chain structure lead to the special properties of Stanyl®. The high crystallization rate, high degree of crystallinity and its melting point of 290 °C result in excellent high-temperature physical and mechanical properties such as: high stiffness, good toughness, high creep and fatigue resistance, high resistance against peak temperatures and high thermal stability. This, combined with the excellent processability i.e. high flow and short cycle times in the injection molding process, has led to the commercial success of Stanyl® in modern electrical, electronic and automotive applications [3–8].

Polyamides absorb water because of the amide functionality [9]. Absorbed water, acting as a plasticizer, lowers the glass transition temperature (T_g) significantly [10–14]. In a preceding paper [15], the mechanism of water uptake by PA46 was demonstrated by means of solid state NMR and magnetic resonance imaging (MRI) relaxometry. It describes a gradual decrease in the amount and the mobility of the absorbed water molecules from the surface towards the core part of water saturated injection molded PA46 plates, originating from a decrease in the cooling rate from the surface to the core during injection molding. MRI projections revealed the distribution profile to be horn-shaped, with a maximum at the surface layers of the plates.

In this paper, PA46 and copolymers of PA46 and PA4*n* (PA46-*co*-PA4*n*, structures shown in Table 1) with 4 mol% of $n = 8$, 12, and 16, are studied by means of thermal analysis, gravimetry, MRI relaxometry and ^{1}H NMR T_2 relaxation experiments. The main goal is to set up a model to predict and tune the effect of incorporation of these linear aliphatic dicarboxylic acid co-monomers on the phase morphology and water uptake of PA46.

* Corresponding author. Tel.: +32-11-26-83-88; fax: +32-11-26-83-01.
E-mail address: jan.gelan@luc.ac.be (J. Gelan).

0032-3861/$ - see front matter © 2004 Elsevier Ltd. All rights reserved.
doi:10.1016/j.polymer.2004.02.007

Table 1
Description of the PA46-*co*-PA4*n* copolymers

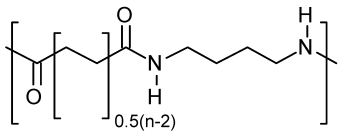

		[CH_2]/[amide] ratio
PA46	100% $n = 6$	4
PA46-*co*-PA48	96% $n = 6$; 4% $n = 8$	4.04
PA46-*co*-PA412	96% $n = 6$; 4% $n = 12$	4.12
PA46-*co*-PA416	96% $n = 6$; 4% $n = 16$	4.20

2. Experimental

2.1. Materials

Pre-polymers were prepared according to patent EP 0254367, example [16]. The pre-polymer particle mass was obtained by adding the dicarboxylic acid(s) (4.95 mol) to a mixture of diaminobutane (5.04 mol) and water (94.5 g) (Table 1). For the copolymers, a mixture of adipic acid (4.752 mol) and the comonomer (0.198 mol) was used. After reaction for 25 min at 207 °C in a closed reactor, the content of the reactor was substantially discharged via a spray nozzle into an area with nitrogen at atmospheric pressure. The resulting pre-polymer particle mass had a water content of 6%.

Pre-polymer powder was charged into a tumble dryer and heated at 230 °C for 24 h in an atmosphere containing 25 wt% water and 75 wt% nitrogen, ensuring a slight gas stream to maintain the right ratio between water and nitrogen over the experiment. The polymer powder was fed to a single screw extruder and injected at a temperature of 305 °C into a mould of 63.5 × 12.7 × 3.4 mm. The mould temperature was set at 80 °C. Plates with a dimension of 30 × 12.7 × 3.4 mm were sawn out and used for MRI and gravimetrical experiments. Annealing was accomplished at 260 °C for 12.5 h under N_2-atmosphere.

2.2. Thermal analysis

DSC scans were performed at a heating rate of 10 °C/min under a nitrogen atmosphere. A sample of 3–5 mg was taken from cryogenically ground polymer. The melting point (T_m) and melting enthalpy (ΔH_m) were determined from the second heating curve, while the crystallization temperature T_c was determined at sample cooling from 330 °C.

2.3. Gravimetric analysis

After drying the plates at 100 °C under N_2-atmosphere for 14 h to constant weight (W_0), they were saturated with water by immersion in distilled water at 50 °C. To study the influence of temperature on the ingress kinetics, the reference sample (PA46) was also saturated at 30 and 70 °C. The plates were removed periodically, dried of excess of water and weighed (W_t). The water uptake was calculated according to Eq. (1) [17], while the diffusion coefficient D (in $mm^2 s^{-1}$) was determined by means of Eq. (2) [18–21],

$$\%\text{water uptake} = \frac{W_t - W_0}{W_0} \times 100 \quad (1)$$

$$\frac{W_t - W_0}{W_{eq} - W_0} = \frac{4}{l\sqrt{\pi}}(Dt)^{1/2} \quad (2)$$

in which W_{eq} represents the weight of the fully equilibrated sample and l the thickness of the plate. Fitting the initial slope of a plot of $(W_t - W_0)/(W_{eq} - W_0)$ vs. $t^{0.5}$ was applied for $(W_t - W_0)/(W_{eq} - W_0) < 0.6$ with negligible deviations from the exact solution of Fick's second low (short-time method) [22]. The activation energy for the diffusion of water in PA46 (E_D) was obtained by means of Eq. (3) [17,23–25], in which R is the gas constant (8.31 J/mol K), D_0 a constant term and T the temperature in Kelvin.

$$\ln(D) = \ln(D_0) - \frac{E_D}{R} \times \frac{1}{T} \quad (3)$$

2.4. Magnetic resonance imaging

MRI images and one-dimensional (1D) projections were acquired at 9.4 T on an Inova 400 Varian vertical bore NMR spectrometer by means of a spin-warp pulse sequence and a micro-imaging probe equipped with a 16 mm coil. All MRI measurements were performed on water saturated plates, which were immobilized in the glass tube by means of a dedicated Teflon holder. A reference capillary, filled with a solution of 0.2% $CuCl_2$ in $H_2O/D_2O = 1/8$, having a short T_1 relaxation time of 0.1 s, was used to normalize the signal intensities of different plates.

The volume-averaged T_1 relaxation times were determined as described before [15]. Since the volume-averaged T_1 relaxation time is approximately the same for all polymers (1.2 s), its value is not further discussed. The T_2 relaxation times were obtained from MRI images as described before [15]. The volume-averaged T_2 decay time (T_2) as well as the spatially resolved T_2 relaxation times in the horn part (outer 0.3 mm) and in the core part (inner 0.3 mm) were determined by means of 1D projections reconstructed from the region between the lines indicated in Fig. 1(a).

2.5. Proton T_2 wideline NMR experiments

Rectangular pieces were placed in a 9 mm NMR tube. After drying in a 50 mbar vacuum oven under nitrogen flow at 70 °C for 70 h, the tube was sealed to protect it from water

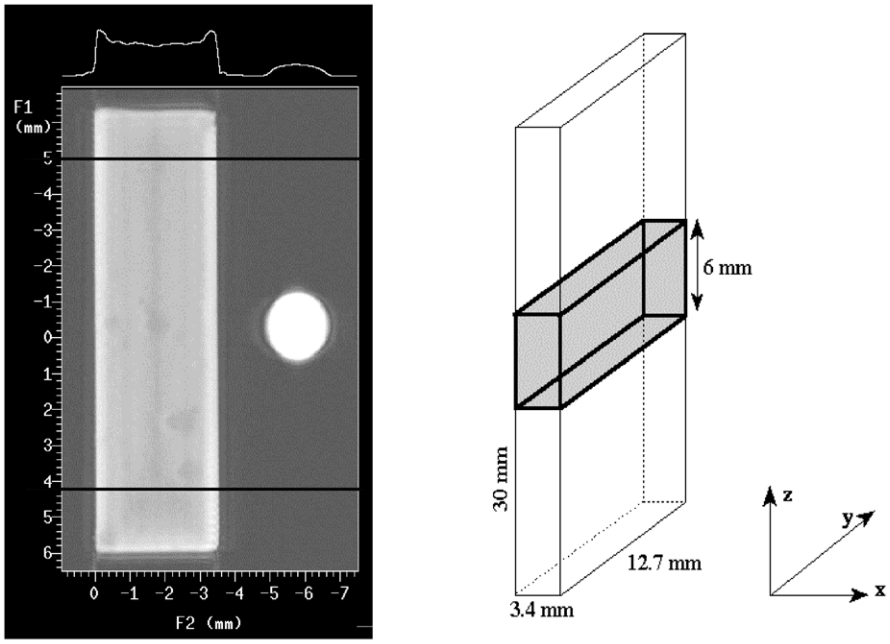

Fig. 1. (a) MRI image (recorded with TE = 1.3 ms) of a water saturated PA46 plate in the presence of a reference capillary filled with doped water. A fixed region, indicated by the two lines, is used to reconstruct the 1D projections. The signal of water in the reference capillary is shown on the right. (b) Experimental setup: size and position of the polyamide plates with respect to the B_0-field (z-direction) of the magnet.

ingress. Proton T_2 relaxation experiments were performed on a Bruker Minispec MQ-20 spectrometer, operating at a proton resonance frequency of 20 MHz. The length of the 90° pulse and the dead time were 2.8 and 7 μs, respectively.

The solid-echo pulse sequence (SEPS), $90°_x - t_{SE} - 90°_y - t_{SE}$-[acquisition of the amplitude of the transverse magnetization $M(t)$], with $t_{SE} = 10$ μs was used to record the free induction decay (FID). The time from the beginning of the first pulse $t = 2(t_{SE} + t_{90})$ was taken as zero, where t_{90} is the duration of the 90° pulse.

The T_2 relaxation times were obtained by performing a least squares fit of the data using (a) the Weibull function [26] (at temperatures <80 °C); (b) a linear combination of a Weibull and exponential function (at temperatures ≥ 80 °C and <120 °C); and (c) a linear combination of a Weibull and two exponential functions (at temperatures ≥ 120 °C) (Eq. (4)):

$$M(t) = M_0^{s} \times \exp[-(t/T_2^{s})]^{\alpha} + M_0^{i} \times \exp[-t/T_2^{i}] + M_0^{l} \times \exp[-t/T_2^{l}] \quad (4)$$

where $\alpha = 1.90 \pm 0.05$. The relative fraction of the relaxation components, as designated in the text by $\%T_2^{index} = (M_0^{index}/[M_0^{s} + M_0^{i} + M_0^{l}]) \times 100\%$, represents the fraction of protons in phases with different molecular mobility, where superscripts 's', 'i' and 'l' stand for short, intermediate and long decay time.

3. Results

The phase structure was thermally characterized by DSC to obtain the melting point, crystallization point and melt enthalpy. ^{1}H wideline NMR T_2 relaxation measurements were performed to obtain information about the relative content of mobile, semi rigid and rigid phase, while MRI measurements allowed studying the spatial distribution of water, the local water mobility and the effect of annealing. Gravimetric experiments provided the diffusion constants and equilibrium water uptake.

3.1. Thermal characterization

Table 2 presents the thermal characteristics of the polyamides measured by DSC. With respect to PA46, the melting points (T_m) of the copolymers PA46-*co*-PA4*n* are all 5 °C lower, indicating that the molar concentration of the comonomer determines the decrease of the melting temperature. Within the copolymer series, there seems to

Table 2
Thermal characteristics of the polyamides

PA46-*co*-PA4*n*	T_m (°C)	T_c (°C)	ΔH_m (J/g)
PA46	290	268	91
PA46-*co*-PA48	285	262	89
PA46-*co*-PA412	285	263	91
PA46-*co*-PA416	285	264	87

be a slight increase in crystallization temperature (T_c) with increasing comonomer length, suggesting that an increase of n results in an increased crystallization rate. A possible explanation is that an enhanced mobility of the PA46 segments in the copolyamide melt is realized in case a longer aliphatic unit is attached that lacks the ability of hydrogen bonding. It is known that increasing the content of CH_2 units in a polyamide lowers the glass transition temperature T_g, which, with equal T_m, explains a higher mobility of the PA46 segments with increasing n.

3.2. Proton T_2 relaxation with respect to molecular mobility and phase composition

Proton wideline NMR T_2 relaxation experiments offer a valuable tool for the analysis of microphase structure and molecular motions in semicrystalline polymers [27–31]. At temperatures well above the glass temperature (T_g), the T_2 relaxation decay can be decomposed into three components which originate from a crystalline phase, a semirigid crystal-amorphous interphase and a soft amorphous phase. In many respects, the intermediate phase has a kinetic origin and may not be considered as a true thermodynamical phase. Apparently, the definition of an interface or a semirigid fraction of the amorphous phase is more appropriate for the phase with intermediate molecular mobility. The distinct T_2 relaxation suggests a significant difference in chain mobility in the different phases due to a fast loss of restrictions on rotational and translational chain mobility when moving away from the crystalline phase. The NMR relaxation method provides a crystallinity value, which is usually in good agreement with that measured by other techniques. It is noted that the phase composition, as determined by the NMR method, is affected to some extent by the temperature of the experiment and the fitting function used for the deconvolution of the FID into separate components.

In order to find out the most suitable temperature for the characterization of the phase composition for PA46 and its copolymers, the ^1H T_2 relaxation behavior was measured as a function of temperature for PA46 (Fig. 2(a) and (b)). The FID below 80 °C can be described with a single relaxation time (T_2^s), which value is typical for crystalline and glassy amorphous materials. A second relaxation component with a longer decay time appears at 80 °C. This temperature corresponds to the glass transition temperature of PA46 [15], causing an increase in T_2 for the least constrained chain fragments in the amorphous phase. Upon increasing temperature, the fraction of rigid material that is composed of crystalline and rigid amorphous phase, decreases at the expanse of the semirigid amorphous phase. Above 120 °C, the FID can be described by three distinct components. The value of T_2 for the third relaxation (T_2^l) is significantly longer compared to T_2^i and is assigned to the most mobile fraction of the amorphous phase. Upon further temperature increase, the fraction of this relaxation component increases at the expense of the semirigid amorphous phase, whereas

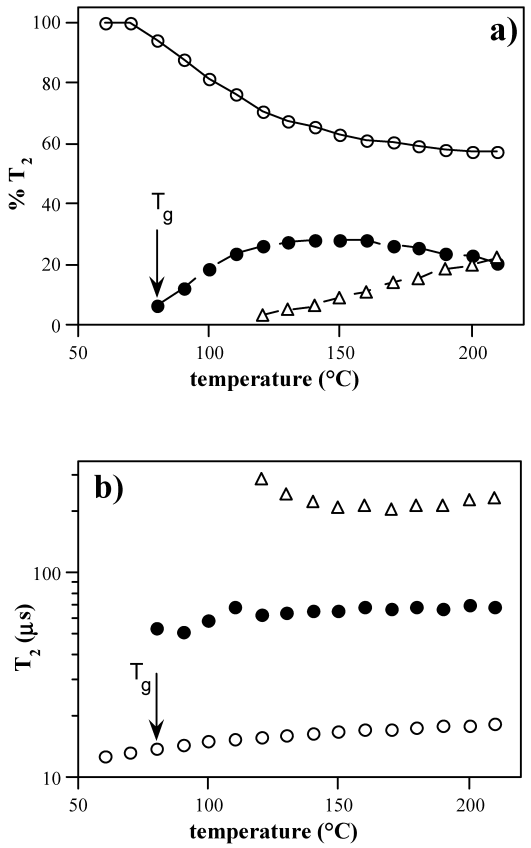

Fig. 2. Temperature dependence of the amount of PA46 fractions with different molecular mobility (a) and the T_2 relaxation time corresponding to these fractions (b). The different components are denoted as short (○), intermediate (●) and long (△). Arrows denote the glass transition temperature.

the rigid fraction of PA46 reaches nearly a constant value above 180 °C. It appears that above this temperature, the T_2^s, T_2^i and T_2^l relaxation components largely originate from the relaxation of crystalline phase, semirigid crystal-amorphous interface and soft amorphous phase, respectively. The relative fractions of these components, $\%T_2^s$, $\%T_2^i$ and $\%T_2^l$, represent the hydrogen content in these phases. The T_2 relaxation parameters at 200 °C are compared for all samples in Table 3. No large difference in molecular mobility in the different phases is observed among the samples.

The crystallinity as determined by the NMR method is

Table 3
Proton T_2 relaxation parameters for the polyamides at 200 °C

	$n = 6$ (PA46)	$n = 8$	$n = 12$	$n = 16$
T_2^s (μs)	18.0 ± 0.1	18.0 ± 0.1	18.1 ± 0.1	18.0 ± 0.1
T_2^i (μs)	72 ± 4	65 ± 4	73 ± 4	66 ± 3
T_2^l (μs)	244 ± 9	224 ± 7	263 ± 8	250 ± 7
$\%T_2^s$	56.7 ± 1	52.8 ± 1	54.3 ± 1	53.0 ± 1
$\%T_2^i$	23.1 ± 1	21.4 ± 1	23.5 ± 1	22.0 ± 1
$\%T_2^l$	20.2 ± 1	25.8 ± 1	22.2 ± 1	25.0 ± 1

Errors indicate the 95% confidence interval of the least square fits.

about 57% for PA46, which is comparable with a crystallinity of 60–70% found for a typical injection molded PA46 sample determined by WAXD [32]. Table 3 also demonstrates that, compared to PA46, the content of the crystalline phase in the copolyamides is a few percents lower with no variation with the chain length n within experimental error. The slight decrease in the crystallinity ($\%T_2^s$), suggests that comonomer chain units are rejected from the crystalline phase. Also the fraction of the most mobile amorphous phase ($\%T_2^l$) seems to be slightly larger for the copolyamides as compared to PA46.

3.3. Diffusion kinetics of water

Gravimetrical results (Table 4), show a significant difference in equilibrium water uptake and rate of water sorption for the different polyamides. Fig. 3 shows the normalized water uptake data $(W_t - W_0)/(W_{eq} - W_0)$ against the square root of time. The linearity of the initial stage of the water uptake indicates a Fickian diffusion [13,33] and allows determining the average diffusion coefficient from the initial slope. The amount of absorbed water and its diffusion coefficients significantly decrease with increasing chain length of the comonomer in the copolyamide series (Table 4). Compared to PA46, only the copolyamide PA46-*co*-PA416 shows a strong reduction in water uptake and diffusion rate.

A large change in water absorption is observed upon annealing the polyamide plates as demonstrated in Fig. 4 and Table 5. Annealing strongly reduces the equilibrium amount of water uptake and the water ingress rate, which both decrease with increasing chain length of the incorporated comonomer. However, compared to the very large reduction in water uptake for PA46 (factor 3.1), the copolyamides show a somewhat less pronounced drop in water uptake (about a factor 2.5).

Table 4
Results obtained by gravimetry and MRI relaxometry for water saturated PA46 and PA46-*co*-PA4*n* plates. $\langle T_2 \rangle$ represents the volume-averaged T_2 decay time, while T_2 horn and T_2 core are determined in a layer of 0.3 mm thickness at the surface and the middle part of the plates, respectively. Spin density values (M_0) are all normalized to 100 for the copolymer PA46-*co*-PA48

	$n = 6$ (PA46)	$n = 8$	$n = 12$	$n = 16$
Water uptake (wt%)	11.7 ± 0.1	12.5 ± 0.1	10.8 ± 0.1	9.6 ± 0.1
D (mm^2s^{-1})	4.1×10^{-6}	4.8×10^{-6}	4.1×10^{-6}	3.4×10^{-6}
$\langle T_2 \rangle$ (ms)	2.8 ± 0.1	3.1 ± 0.1	2.2 ± 0.1	1.9 ± 0.1
$\langle M_0 \rangle$	92 ± 3	100 ± 2	87 ± 2	77 ± 3
T_2 horn (ms)	3.2 ± 0.1	3.6 ± 0.1	2.4 ± 0.1	2.0 ± 0.1
M_0 horn	78 ± 2	100 ± 2	73 ± 2	46 ± 2
T_2 core (ms)	2.5 ± 0.1	2.7 ± 0.1	2.0 ± 0.1	1.8 ± 0.1
M_0 core	87 ± 2	100 ± 2	79 ± 2	55 ± 3
T_2 horn/T_2 core	1.28	1.33	1.20	1.11
M_0 horn/M_0 core	0.90	1.00	0.92	0.84

Errors indicate the 95% confidence interval of the least square fits.

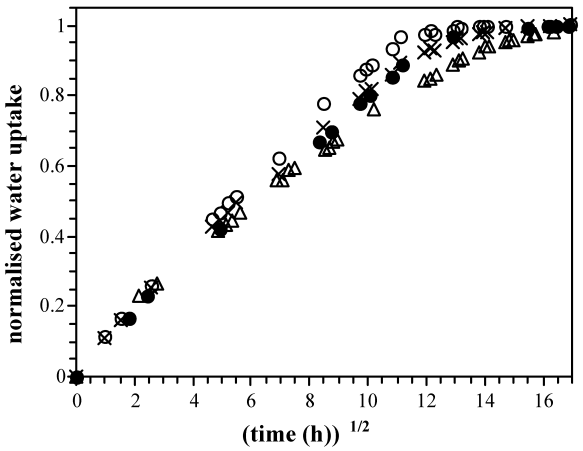

Fig. 3. Normalized water uptake at 50 °C as a function of square root of time for PA46 (●) and the PA46-*co*-PA4*n* copolymers with $n = 8$ (○), $n = 12$ (×) and $n = 16$ (△).

Fig. 5 shows the influence of temperature on the water ingress in PA46. As expected, the water ingress rate becomes higher upon raising the temperature as demonstrated by the diffusion coefficients presented in Table 6. An activation energy of diffusion, E_D, of 46.8 kJ/mol is obtained by fitting according to Eq. (3). This is comparable with the values found in literature for PA6 (35 kJ/mol) [34] and PA66 (60 kJ/mol) [35]. In agreement with literature [36,37], the equilibrium water uptake drops slightly upon raising the temperature, indicating a thermal dependency of the polymer/solvent interactions. Within the 40 °C temperature range used in this study, the temperature dependence of the solubility coefficient S (in g water/g polymer) follows an Arrhenius-type relationship:

$$S = S_0 \times \exp(-\Delta H_S/RT) \quad (5)$$

A plot of the logarithm of the solubility as a function of reciprocal temperature yields the partial molar heat of solution, $\Delta H_S = -1.5$ kJ/mol, indicating an exothermic

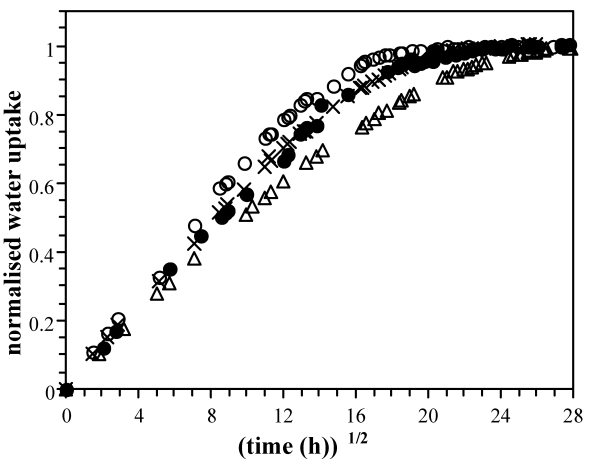

Fig. 4. Normalized water uptake at 50 °C as a function of square root of time for annealed PA46 (●) and annealed PA46-*co*-PA4*n* copolymers: $n = 8$ (○), $n = 12$ (×) and $n = 16$ (△).

Table 5
Gravimetric results for annealed water saturated PA46 and PA46-*co*-PA4*n* copolymer plates

	$n = 6$ (PA46)	$n = 8$	$n = 12$	$n = 16$
Water uptake (wt%)	3.8 ± 0.1	5.3 ± 0.1	4.0 ± 0.1	3.8 ± 0.1
D (mm^2s^{-1})	2.1×10^{-6}	2.9×10^{-6}	2.1×10^{-6}	1.9×10^{-6}

Errors indicate the 95% confidence interval of the least square fits.

sorption and explaining the decrease in solubility with increasing temperature [38].

3.4. MRI relaxometry

MRI experiments on water saturated plates were performed in order to obtain information about the spatial distribution of water and its molecular mobility. Fig. 1 shows the image of a water saturated PA46 plate. The reconstructed 1D projections of regular PA46 and the different copolymers are presented in Fig. 6(a)–(d). Although the plates are saturated to equilibrium, all polyamides reveal a horn-shaped intensity projection with a gradual decrease of the signal intensity towards the center of the plate. The volume-averaged and spatially resolved spin density values (M_0) and T_2 decay times, being proportional to the amount of water and water molecular mobility respectively, are presented in Table 4. The volume-averaged water molecular mobility and water concentration of PA46 are lower than those of the copolymer with $n = 8$, but, within the copolymer series, both MRI parameters clearly decrease with increasing chain length of the comonomer. The volume-averaged M_0 values correlate well with the amount of water uptake as determined by gravimetry. The spatially dependent M_0 and T_2 values demonstrate a similar behavior. As shown in Fig. 6 and Table 4, the relative intensity ratio between horn and core (M_0 horn)/(M_0 core) decreases with increasing chain length of the incorporated comonomer.

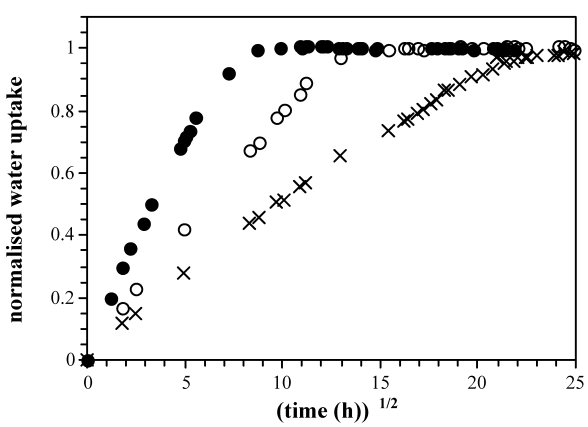

Fig. 5. Normalized water uptake at 30 °C (×), 50 °C (○) and 70 °C (●) for PA46 as a function of square root of time.

Table 6
Gravimetric and MRI relaxometry results for water saturated PA46 as a function of temperature. $\langle T_2 \rangle$ represents the volume-averaged T_2 decay time

	$T = 30$ °C	$T = 50$ °C	$T = 70$ °C
Water uptake (wt%)	12.2 ± 0.1	11.7 ± 0.1	11.4 ± 0.1
D (mm^2s^{-1})	1.5×10^{-6}	4.1×10^{-6}	12.7×10^{-6}
$\langle T_2 \rangle$ (ms)	2.4 ± 0.1	2.8 ± 0.1	2.9 ± 0.1
T_2 horn (ms)	2.6 ± 0.1	3.2 ± 0.1	3.7 ± 0.1
T_2 core (ms)	2.2 ± 0.1	2.5 ± 0.1	2.3 ± 0.1
T_2 horn/T_2 core	1.18	1.28	1.61

Errors indicate the 95% confidence interval of the least square fits.

Annealing results in a strong decrease of the signal intensity in the MRI images as shown in Fig. 6(e). The profile of the projection is no longer horn-shaped but becomes almost rectangular. The mean volume-averaged T_2 relaxation time of the annealed polyamides is strongly reduced to about 0.64 ms.

MRI relaxation results, performed as a function of temperature on PA46, are presented in Table 6. With increasing temperature, a slight increase in the molecular mobility of the absorbed water molecules, represented by the T_2 decay time, is observed but only at the surface of the plates. The T_2 value for the inner core seems to be more or less independent of temperature.

4. Discussion

In order to obtain a better understanding of the water uptake behavior of polyamides in general, a combination of different factors, all influencing the water uptake, is discussed.

4.1. Influence of the hydrophobicity, as determined by the [CH_2]/[amide] ratio and the amount of crystallinity

It has already been established in literature that an increase in the molar ratio [CH_2]/[amide] results in a decrease of the equilibrium water uptake [14,37]. The curve presented by the open symbols in Fig. 7 demonstrates this hydrophobic effect for different homopolymers PA*xn* with *x* and *n* being even numbers [39], and for the three copolyamides PA46-*co*-PA4*n*. The copolymer PA46-*co*-PA48 is situated slightly above the curve of the homopolymers PA*xn* (and absorbs more water than PA46; Table 1) while the copolymers with $n = 12$ and 16 are situated under the curve.

However, since water is only absorbed by the amorphous phase [40–42], differences in crystallinity might also effect the position of the copolymers with respect to the curve for the homopolymers in Fig. 7. The crystallinity of PA46 is known to be substantially higher than that of polyamides with higher [CH_2]/[amide] ratios, e.g. because of its high symmetrical chain structure. To rule out the differences in

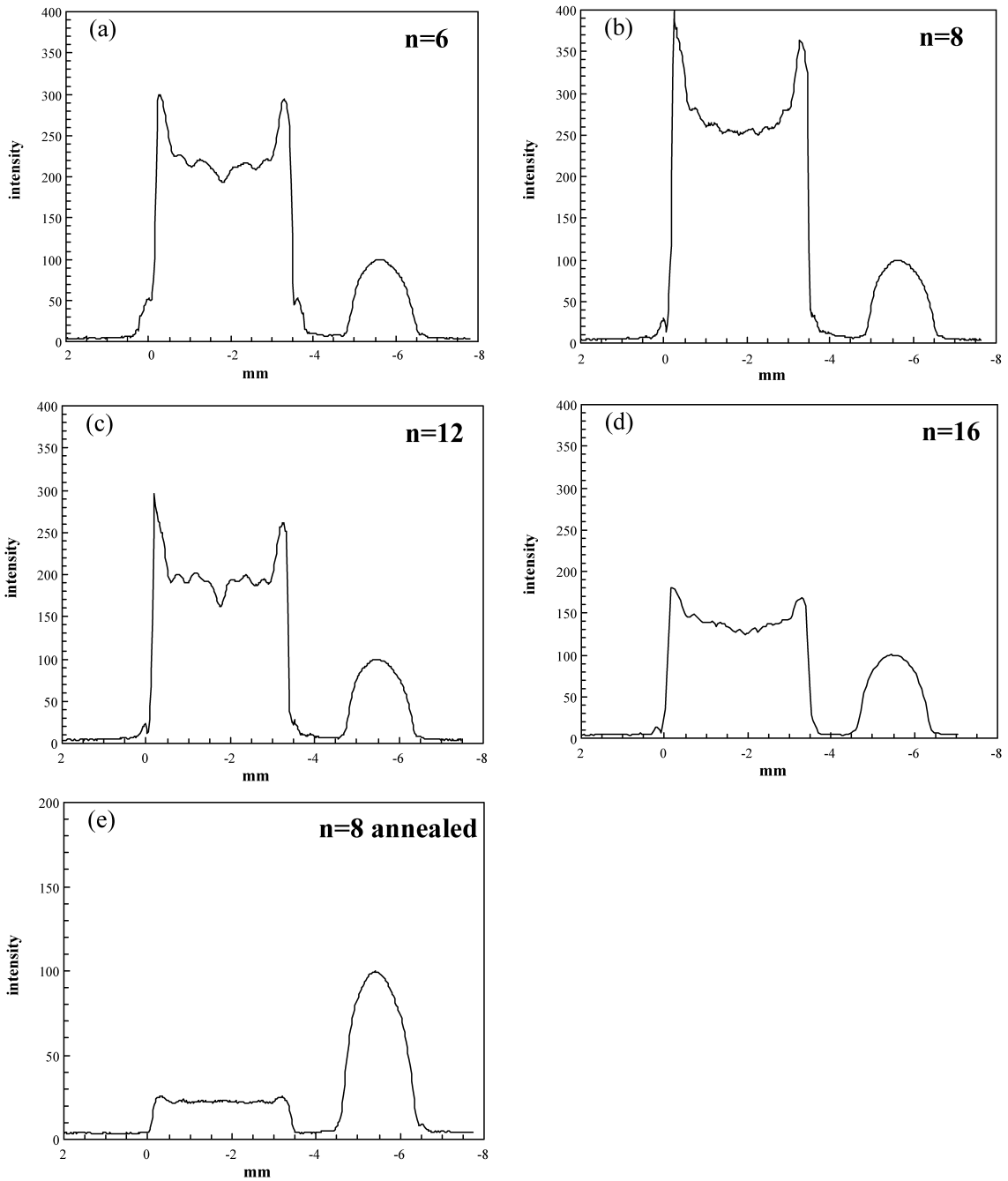

Fig. 6. 1D projections of the images (TE = 1.3 ms) of water saturated PA46 (a) and PA46-*co*-PA4*n* plates: $n = 8$ (b), $n = 12$ (c) and $n = 16$ (d), and for $n = 8$ after annealing (e). The signal of doped water in the reference capillary is shown on the right.

amount of crystallinity, the water uptake in the amorphous phase of PA46 and the copolyamides is calculated by using the data of Table 3, accepting that $\%T_2^s$ represents the fraction of the crystalline phase. Assuming a crystallinity of 50% for the other PA*xn* polyamides [43], the filled symbols shown in Fig. 7 are obtained. While the water uptake for the copolymer PA46-*co*-PA48 can be reasonably well explained by the hydrofobicity and crystallinity, the copolymers with $n = 12$ and 16 are still not situated on the curve of the homopolymers. This means that the hydrophobic effect and the differences in amount of crystallinity cannot completely explain the water uptake of these two copolymers.

4.2. Annealing

Annealing results in a large decrease of the amount of absorbed water and of the molecular mobility of the absorbed water (Table 5). Since it is known that water is only absorbed by the amorphous phase [40–42] and that the amount of crystallinity of PA46 is not influenced

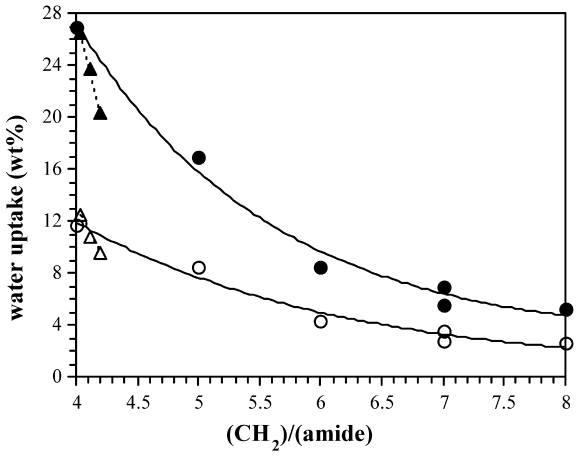

Fig. 7. Equilibrium water uptake of even–even homopolyamides PA*xn* (○, ●) and of the copolyamides PA46-*co*-PA4*n* (△, ▲). Open symbols represent equilibrium water uptake; filled symbols represent equilibrium water uptake of the amorphous phase.

significantly by annealing [44], the observed reductions in water uptake and water mobility can only be explained by a closer coupling of the amide groups in the amorphous phase after annealing. For PA46, such an increase in the density of the amorphous phase was already demonstrated by density measurements in a previous publication [15].

The more pronounced reduction in water uptake upon annealing for PA46 as compared to the copolymers, i.e. a 3.1 fold vs. about a 2.5 fold reduction, can be explained by the high symmetric chain structure of PA46. For the copolymers, the comonomer units decrease the ability for hydrogen bond formation between amide groups in adjacent chains, explaining the smaller reduction in water uptake upon annealing. The strongly reduced volume-averaged T_2 decay time (0.64 ms) observed after annealing confirms that, not only the amount of amorphous phase but mainly the inter-chain interactions in the amorphous phase determine the amount, ingress rate and molecular mobility of absorbed water.

4.3. Crystallization rate and temperature-time history

The high crystallization rate of PA46 compared to other polyamides lays in its high symmetry and low [CH_2]/[amide] ratio [39]. Since crystallites hinder translational mobility in the amorphous phase, it was suggested in a previous paper [15] that, starting from the melt, the faster cooling of the outer layer in the mould (thermal gradient) results in a more kinetically controlled morphology of the amorphous phase in this layer. This hampers the hydrogen bond formation between adjacent chains, resulting in a gradual increase of the mean distance between the amide groups in the amorphous phase towards the surface of the plates. As a result, a gradual increase in the amount and mobility of water molecules arises from the center to the outside of the plates that can be visualized by the horn-shaped water distribution profiles in the MRI projections as shown in Figs. 1 and 6.

For the copolymer series, the increasing values of T_c, with constant T_m (Table 2), suggest that the crystallization rate becomes faster with increasing n. This should lead to more pronounced horn-shaped water distribution profiles (more kinetically controlled morphology) in the copolymer series. Surprisingly a decreasing ratio (M_0 horn)/(M_0 core) is found with increasing n (Table 4). Therefore, also the molecular mobility of the chain segments is taken into account.

4.4. Mobility of the copolymer segments in PA46-*co*-PA4*n*

A reasonable explanation for the increasing value of T_c with increasing n lies in an enhanced mobility of PA46 segments linked by the long comonomer units. Thus the comonomer units should be seen as spacer groups, obstructing the formation of H-bonds between adjacent chains and increasing the local chain mobility of PA46 fragments in the copolymer. This less constrained chain mobility results in a closer chain packing in the amorphous phase (more thermodynamical control), while at the same time enhances the crystallization process. This spacer group effect is especially pronounced for the longer comonomers, elucidating why these copolymers deviate the most from the homopolymer curve in Fig. 7. The effect is minimal for the copolymer PA46-*co*-PA48, clarifying why this copolymer is situated more or less on the hydrophobicity curve in Fig. 7. In conclusion, it can be stated that the length of the comonomer unit can be used to tune the degree of inter-chain amide group coupling. It completely explains the decreasing ratio (M_0 horn)/(M_0 core) and the decrease in water mobility (ratio (T_2 horn)/(T_2 core)) with increasing n value as observed by MRI, and the deviation of the copolymers from the homopolymer curve in Fig. 7.

4.5. Dependency of water uptake on temperature

As expected, an increase in the molecular mobility of the absorbed water is observed with increasing temperature. This effect however, is clearly more pronounced for the water molecules situated at the surface of the plates as compared to these in the inner core, for which the T_2 values seem to be more or less independent of temperature (Table 6). These observations confirm the gradual decrease in the density of the amorphous phase towards the surface of the PA46 plates.

5. Conclusion

Gravimetrical experiments show a clear decrease in the equilibrium water uptake and water ingress rate of PA4*n* (PA46-*co*-PA4*n*) with increasing n. The same behavior is observed for the MRI relaxation parameters M_0 and T_2. The

strong decrease in water uptake and water molecular mobility observed after annealing proves that the morphology of the amorphous phase is an important parameter since it determines the strength of the coupling between the inter-chain amide groups. In order to obtain a better understanding of the water uptake behavior of polyamides, several parameters were evaluated. The hydrophobic effect, even corrected for the amount of crystallinity and crystallization rate, does not explain the strong decrease in water absorption observed for the copolymers with long comonomer units ($n = 12$ and 16). The surprisingly large reduction in water uptake of these copolymers (Fig. 7) can only be explained by an enhanced chain dynamics of the PA46 segments linked by the long comonomer units. Upon cooling from the melt, the increased chain mobility of the PA46 segments allows a better structuring and closer coupling of the amide groups in the amorphous phase (less kinetic control). Since this chain mobility enhancement is most pronounced for PA46-*co*-PA416, it accounts for the largest reduction in water uptake and water mobility.

The results demonstrate that modification of PA46 with a hydrophobic comonomer enables to reduce and tune the water uptake in a special but predictable way. An improved model is presented that describes the water uptake in nylons from a more molecular point of view.

Acknowledgements

The authors gratefully acknowledge The Fund for ScientificResearch-Flanders (FWO) and The Belgian Programme on Interuniversity Attraction Poles (IUAP) initiated by the Belgian State, Prime Minister's office for financial support.

References

[1] Carothers WH. US Patent 2,130,948; 1938.
[2] Gaymans RJ, Van Utteren TE, Van Den Berg JWA, Schuyer J. J Polym Sci 1977;15:537.
[3] Roerdink E, Warnier JMM. Polymer 1985;26:1582.
[4] Steeman PAM, Maurer FHJ. Polymer 1992;33:4236.
[5] Kudo K, Mochizuki M, Kiriyama S, Watanabe M, Hirami M. J Appl Polym Sci 1994;52:861.
[6] Suzuki A, Endo A, Kunugi T. J Polym Sci B: Polym Phys 1998;36: 2737.
[7] Bermudez M, Leon S, Aleman C, Munoz-Guerra S. J Polym Sci B: Polym Phys 2000;38:41.
[8] Creemers H. Engng Plast 1989;11:19.
[9] Kawasaki K, Sekita Y. J Polym Sci Part A 1964;2:2437.
[10] Hutchison JL, Murthy NS, Samulski ET. Macromolecules 1996;29: 5551.
[11] Knopp B, Suter UW. Macromolecules 1997;30:6114.
[12] Murthy NS, Akkapeddi MK, Orts WJ. Macromolecules 1998;31:142.
[13] Fyfe CA, Randall LH, Burlinson NE. J Polym Sci A: Polym Chem 1993;31:159.
[14] Razumovskii LP, Markin VS, Zaikov GY. Polym Sci USSR 1985;27: 751.
[15] Adriaensens P, Pollaris A, Carleer R, Vanderzande D, Gelan J, Litivinov VM, Tijssen J. Polymer 2001;42:7943.
[16] Bongers AJP. Stamicarbon patent EP 0254367; 16 July 1987.
[17] Maggana C, Pissis P. J Polym Sci B: Polym Phys 1999;37:1165.
[18] Vahdat N, Sullivan VD. J Appl Polym Sci 2001;79:1265.
[19] Crank J, 2nd ed. The mathematics of diffusion, London: Oxford University Press; 1975.
[20] Rezac ME, John T. Polymer 1998;39:599.
[21] Soles CL, Chang FT, Gidley DW, Yee AF. J Polym Sci B: Polym Phys 2000;38:776.
[22] Crank J, Park GS, Diffusion in polymers, New-York: Academic Press; 1968.
[23] Frisch HL. Polym Engng Sci 1980;20:2.
[24] Sperling LH, Introduction to physical polymer science, New York: Wiley; 1992.
[25] Taraszka JA, Weiss RG. Macromolecules 1997;30:2467.
[26] Ibbett RN, NMR spectroscopy of polymers, Glasgow: Blackie/ Chapman & Hall; 1993.
[27] Fedotov VD, Schneider H. Structure and dynamics of bulk polymers by NMR methods. In: Diehl P, Fluck E, Gunter H, Kosfeld R, Seelig I, editors. NMR basic principles and progress. Berlin: Springer-Verlag; 1989.
[28] McBrierty VJ, Packer KJ, Nuclear magnetic resonance in solid polymers, Cambridge: Cambridge University Press; 1993.
[29] Dadauli D, Hareris RK, Kenwright AM, Say BJ, Sünnetçioglu MM. Polymer 1994;35:4083.
[30] Hansen EW, Kristiansen PE, Pedersen B. J Phys Chem B 1998;102: 5444.
[31] Schreurs S, François JP, Adriaensens P, Gelan J. J Phys Chem B 1999; 103:1393.
[32] Becker GW, Braun D. Kunststoff handbuch: polyamide. München: Carl Hanser; 1998. p. 574.
[33] Chin JW, Nguyen T, Aouadi K. J Appl Polym Sci 1999;71:483.
[34] Hernandez RJ, Gavara R. J Polym Sci B: Polym Phys 1994;32:2367.
[35] Mansfield P, Bowtell R, Blackband S. J Magn Reson 1992;99:507.
[36] Wolf CJ, Bornmann JA, Grayson MA. J Polym Sci B: Polym Phys 1992;30:113.
[37] Fukuda M, Miyagawa M. Hyogo Daigaku Kenkyu Kiyo, Dai-3-bunsatsu 1985;15:125.
[38] de Naylor TdeV. Polymer properties. Permeation properties in comprehensive polymer science, vol. 2. Oxford: Pergamon Press; 1989.
[39] Loo LS, Cohen RE, Gleason KK. Science 2000;288:116.
[40] Hirschinger J, Miura H, Gardner KH, English AD. Macromolecules 1990;23:2153.
[41] Murthy NS, Stamm M, Sibilia JP, Krimm S. Macromolecules 1989; 22:1261.
[42] Eltink S, de Boer S, Moonen J. Crystallinity studies on polyamides. Internal publication, The Netherlands: DSM Research; 1992.
[43] Vieweg/Müller kunststoff handbuch band VI: polyamide. Munich: Hanser; 1996. p. 470.
[44] Xenopoulos A, Clark ES. In: Kohan MI, editor. Nylon plastics handbook. Munich: Carl Hanser Verlag; 1995. p. 125.